

Rapid, High-resolution and Distortion-free R_2^* Mapping of Fetal Brain using Multi-echo Radial FLASH and Model-based Reconstruction*

Xiaoqing Wang¹, Hongli Fan², Zhengguo Tan³, Serge Vasylechko¹, Edward Yang¹, Ryne Didier¹, Onur Afacan¹, Martin Uecker⁴, Simon K. Warfield¹, and Ali Gholipour^{1,5,6}

¹Department of Radiology, Boston Children’s Hospital, Harvard Medical School, Boston, Massachusetts, USA

²Siemens Medical Solutions, Boston, Massachusetts, USA

³Department of Radiology, University of Michigan, Ann Arbor, Michigan, USA

⁴Institute of Biomedical Imaging, Graz University of Technology, Graz, Austria

⁵Department of Radiological Sciences, University of California Irvine, Irvine, California, USA

⁶ Department of Electrical Engineering and Computer Science, University of California Irvine, Irvine, California, USA

January 8, 2025

Abstract

Purpose: To develop a rapid, high-resolution and distortion-free quantitative R_2^* mapping technique for fetal brain at 3 T.

Methods: A 2D multi-echo radial FLASH sequence with blip gradients is adapted for fetal brain data acquisition during maternal free breathing at 3 T. A calibrationless model-based reconstruction with sparsity constraints is developed to jointly estimate water, fat, R_2^* and B_0 field maps directly from the acquired k-space data. Validations have been performed on numerical and NIST phantoms and five fetal subjects ranging from 27 weeks to 36 weeks gestation age.

Results: Both numerical and experimental phantom studies confirm good accuracy and precision of the proposed method. In fetal studies, both the

*Part of this work has been presented at the ISMRM, 2024, Singapore. Another part of this work has been submitted for consideration of presentation at the ISMRM 2025, Honolulu.

parallel imaging compressed sensing (PICS) technique with a Graph Cut algorithm and the model-based approach proved effective for parameter quantification, with the latter providing enhanced image details. Compared to commonly used multi-echo EPI approaches, the proposed radial technique shows improved spatial resolution ($1.1 \times 1.1 \times 3 \text{ mm}^3$ vs. $2\text{-}3 \times 2\text{-}3 \times 3 \text{ mm}^3$) and reduced distortion. Quantitative R_2^* results confirm good agreement between the two acquisition strategies. Additionally, high-resolution, distortion-free R_2^* -weighted images can be synthesized, offering complementary information to HASTE.

Conclusion: This work demonstrates the feasibility of radial acquisition for motion-robust quantitative R_2^* mapping of the fetal brain. This proposed multi-echo radial FLASH, combined with calibrationless model-based reconstruction, achieves accurate, distortion-free fetal brain R_2^* mapping at a nominal resolution of $1.1 \times 1.1 \times 3 \text{ mm}^3$ within 2 seconds.

Keywords: R_2^* mapping, fetal MRI, distortion-free, multi-echo radial FLASH, model-based reconstruction

1 Introduction

Quantitative R_2^* (where $R_2^* = 1/T_2^*$) mapping of the fetal brain is of increasing value. For example, changes in R_2^* values across gestational age provide a quantitative measure of early brain development [1]. Furthermore, R_2^* mapping and R_2^* -weighted imaging are valuable in identifying intracranial hemorrhage in the fetal brain [2, 3]. The quantitative values are also playing an important role for optimizing R_2^* -weighted functional fetal MRI [4–6]. However, obtaining accurate and high-resolution R_2^* imaging of the fetal brain is challenging due to motion caused by maternal respiration and unpredictable fetal movements [7, 8]. As a result, single-shot sequences, particularly single-shot 2D multi-echo Echo-Planar Imaging (EPI)-based approaches [1, 5, 9–12], are typically used for R_2^* quantification of fetal brain. These techniques were initially developed for 1.5 T [1] and 3.0 T [5, 9], with recent adaptations for 0.55 T [13]. While relatively higher resolution and signal-to-noise ratio (SNR) imaging is achievable at higher fields, low field (e.g., 0.55 T) imaging has shown reduced distortion artifacts for the EPI readout [14], which is attributed to reduced field inhomogeneity and smaller R_2^* s (i.e., longer T_2^* s). Consequently, quantitative R_2^* mapping of fetal body organs has also been reported at 0.55 T [15].

Despite the scan efficiency of EPI, its prolonged readout makes EPI susceptible to geometric distortion caused by B_0 field inhomogeneity, particularly at higher field strengths. Additionally, the extended readout time necessitates a trade-off between imaging speed (short echo times) and spatial resolution due to T_2^* decay in the multi-echo EPI sequence [16]. For instance, the commonly reported spatial resolution for fetal brain imaging is $3 \times 3 \times 3 \text{ mm}^3$ [5, 9, 11], which may limit its usefulness in clinical diagnosis where high-resolution imaging is required [2, 3, 8, 17].

Radial acquisition is an alternative sampling strategy that has gained significant interest in the past decade due to its tolerance to data undersampling

and robustness against motion [18–21]. It has been applied to imaging children with reduced sedation [22–24] and in free-breathing fetal studies [25–27]. Stack-of-stars multi-echo radial fast low-angle shot (FLASH) sequence has also been used for quantitative R_2^* mapping in adult abdominal imaging [28–31] and the fetal placenta [27]. However, the unpredictable motion of the fetal brain, combined with maternal motion and motion-induced phase errors, poses significant challenges for applying 3D sequences to quantitative imaging of the fetal brain.

Alongside motion-robust sequence design, advanced image reconstruction is essential for efficient quantitative imaging. Reconstruction techniques that incorporate prior signal model information to constrain parameter space have been developed [32–38]. Among these, nonlinear model-based reconstruction techniques [38, 39] are highly efficient. These techniques incorporate complex spin dynamics directly in the reconstruction. By formulating reconstruction as a nonlinear inverse problem, model-based reconstruction can estimate physical quantitative maps from undersampled k-space data without intermediate reconstruction or pixelwise fitting. Advanced regularization techniques, such as sparsity constraints [40], further enhance precision in quantitative mapping. Recently, this approach has been extended to reconstruct water, fat, and R_2^* maps from undersampled 3D multi-echo FLASH for liver imaging [28, 41], also enabling additional B_0 estimation [30].

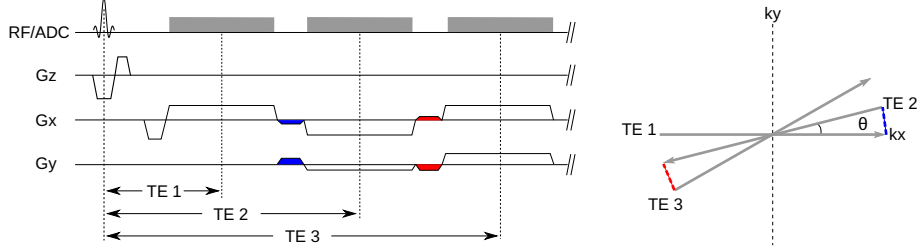
Building on the ideas above, this work aims to develop a rapid quantitative R_2^* mapping of fetal brain utilizing a 2D multi-echo radial FLASH sequence with blip gradients and a calibrationless nonlinear model-based reconstruction. While the radial sequence provides motion robustness and efficient k-space coverage for fetal imaging, the model-based reconstruction estimates quantitative maps directly from undersampled k-space, reducing the number of unknowns in the estimation process. This combination enables high-resolution and distortion-free quantitative R_2^* mapping ($1.1 \times 1.1 \times 3 \text{ mm}^3$) of fetal brain in **two seconds per slice**. Validations have been performed on numerical simulations, experimental phantom, and five fetuses each scanned at an age between 27 to 36 weeks of gestation.

Methods

Sequence Design

A 2D multi-echo radial FLASH sequence is adapted for data acquisition. Similar to [42], radial spokes are designed to rotate along the echo dimension using blip gradients, enabling an efficient k-space coverage (Supporting Information Figure S1). The distribution of spokes is designed in a way that radial lines from several excitations (e.g., 3) and all echoes are equally distributed [42] in one k-space, with an angle $\theta_{l,m} = 2\pi / (N_E \cdot N_S) \cdot [(l-1) \cdot N_E + m - 1]$ for the l th TR and the m th echo. N_E and N_S are the number of echoes and shots (TRs) per k-space, respectively. Spokes acquired in consecutive k-space frames are then rotated by a small golden-angle ($\approx 68.75^\circ$) with respect to the previous

one [43] to enable a complementary coverage of k-space. Since the R_2^* values of fetal brain are reported to be much smaller than those of adult brains [4], the number of echoes is extended from 7 [44] to 35 to enable a robust R_2^* estimation.



Supporting Information Figure S1. Schematic diagram of the 2D multi-echo radial FLASH sequence (three echoes are shown). Blip gradients (blue and red regions) are introduced among echoes to enable a complementary k-space coverage. θ is determined in a way that spokes from all echoes and 3 TRs are equally distributed. I.e., with 35 echoes and 3 TRs, $\theta = 360^\circ / (35 \times 3)$.

Signal Equation and Model-based Reconstruction

Although the fetal brain contains minimal fat, surrounding tissues, such as maternal body tissue, include fat. To account for this, we construct the signal equation as follows [30]:

$$M_{TE_m} = (W + F \cdot z_m) \cdot \exp(TE_m \cdot i2\pi \cdot f_{B_0}) \cdot \exp(-TE_m \cdot R_2^*) \quad (1)$$

with W and F being the water and fat components, respectively; z_m is the summarized 6-peak fat spectrum [45] at echo time TE_m ; and f_{B_0} and R_2^* are the corresponding field map and relaxation rate, respectively. The estimation of the unknowns $(W, F, R_2^*, f_{B_0})^T$ is then formulated as a nonlinear inverse problem; i.e., by combining the above physical model with the parallel imaging equation [46, 47], we construct a nonlinear forward operator F , which maps the unknowns in Equation (1) and the unknown coil sensitivities C to the acquired multi-channel data y at TE_m , i.e.,

$$F : x \mapsto y = \mathcal{P}\mathcal{F}C \cdot M_{TE_m}(x_p) . \quad (2)$$

Here, \mathcal{P} is the sampling pattern and \mathcal{F} is the Fourier transform. By defining $x_c = (c_1, \dots, c_k, \dots, c_K)^T$, with c_k the individual k th coil sensitivity map, the vector of unknowns in Equation (2) is $x = (x_p, x_c)^T$. The estimation of x is then formulated as an optimization problem, i.e.,

$$\hat{x} = \operatorname{argmin}_{x \in D} \frac{1}{2} \sum_{TE} \| \mathcal{P}\mathcal{F}C \cdot M_{TE_m}(x) - Y_{TE_m} \|_2^2 + R(x) . \quad (3)$$

Here, D is a convex set, ensuring non-negativity of R_2^* . $R(\cdot)$ is the regularization term for both parameter maps and coil sensitivity maps. In particular, we use

joint ℓ_1 -Wavelet sparsity constraint [48] on $(W, F, R_2^*)^T$ to exploit sparsity and correlations between maps and Sobolev regularization on the f_{B_0} map [30, 44] and the coil sensitivity maps [47] to enforce smoothness. The above optimization problem is solved by IRGNM-FISTA [48] using the Berkeley Advanced Reconstruction Toolbox (BART) [49]. More details for IRGNM-FISTA can be found in Ref. [48].

Numerical Simulations

To validate the accuracy of the proposed approach, a numerical phantom with ten circular tubes and a background was simulated. The R_2^* values were set to be from 10 s^{-1} to 200 s^{-1} (i.e., T_2^* from 10 ms to 200 ms with a step size of 20 ms). The off-resonance ranged from -50 Hz to 50 Hz with a step size of 10 Hz. The fat fraction was set to be 20% for all tubes and backgrounds. The k-space data was derived from the analytical Fourier representation of an ellipse assuming an array of eight circular receiver coils surrounding the phantom. The 2D multi-echo radial FLASH sequence described in the sequence design section was used to sample the simulated k-space with a base resolution of 192 pixels covering a field of view of 128 mm. The other sequence parameters are the same as those listed in the following Experiments section. Complex white Gaussian noise with a standard deviation of 0.1 was added to the simulated k-space data.

Experiments

All MRI experiments were conducted on a Magnetom Prisma 3T scanner (Siemens Healthineers, Erlangen, Germany) during maternal free breathing. The study was approved by the Institutional Review Board, and written informed consent was obtained from all participants. Validation was first performed using the T_1 spheres of a NIST phantom [50]. Phantom scans employed a 64-channel head/neck coil, while fetal imaging utilized a 30-channel abdominal coil. Five pregnant female subjects (29 ± 7 years old; fetuses: 32.6 ± 3.6 weeks) without known illness were enrolled and scanned. Standard Half Fourier Single-shot Turbo spin-Echo (HASTE) images were acquired first for each subject in three (axial, coronal, and sagittal) orientations with a FOV of $256 \times 256 \text{ mm}^2$, matrix size = 256×256 , slice thickness = 2 mm, and a total acquisition time of 1-1.5 second per slice. Radial fetal scans were performed with the following acquisition parameters: FOV = $256 \times 256 \text{ mm}^2$, matrix size = 224×224 , slice thickness = 3 mm, 35 echoes with TR = 68.3 ms, $TE_1/\delta TE/TE_{35} = 2.37/1.88/66.90$ ms, FA = 20° , bandwidth = 740 Hz/pixel, and 30 RF excitations with 1050 radial acquired spokes for all echoes. The multi-echo EPI images were acquired for quantitative comparison. The parameters for EPI were: FOV = $256 \times 256 \text{ mm}^2$, matrix size = $96\text{-}128 \times 96\text{-}128$, slice thickness = 3 mm, TEs = (23.4-29.8, 74.90-77.48, 126.38-147.20, 177.88-207.46) ms. Repeated radial scans were able to be conducted on three subjects to assess repeatability of the proposed method.

Additionally, for the phantom study, a vendor-provided 3D Cartesian multi-echo sequence was used for reference with these parameters: FOV = 256×256 mm², matrix size = 224×224 , slice thickness = 3 mm with 30 slices, 11 echoes with TR = 65 ms, TE₁/δTE/TE₁₁ = 6.0/5.5/61.0 ms, FA = 15°, bandwidth = 300 Hz/pixel, and acceleration factor 2. The total acquisition time was 4:17 min.

Iterative Reconstruction

All iterative reconstructions were performed offline using BART [49]. The multi-echo radial FLASH datasets from multiple receiver coils were first corrected for gradient delay errors using RING [51] and then compressed to 12 virtual coils via principal component analysis. The data and sampling trajectory were subsequently gridded onto a Cartesian grid, where all iterative steps were carried out using FFT-based convolutions with the point-spread function [52, 53]. The model-based iterative reconstruction was executed on a GPU with 48 GB of memory (RTX A6000, NVIDIA, Santa Clara, CA), with a computation time of 5–10 minutes per dataset. For comparison, the same multi-echo datasets were jointly reconstructed using the parallel imaging and compressed sensing (PICS) method, with coil sensitivity maps estimated from the first echo and joint sparsity constraints applied across spatial and echo dimensions. After image reconstruction, quantitative water, fat, R_2^* , and B_0 maps were estimated using the Graph Cut technique [54], available in the ISMRM water-fat toolbox [55].

Quantitative Analysis

All quantitative results are reported as mean ± standard deviation (SD). Regions-of-interest (ROIs) were carefully drawn into the frontal white matter (FWM), thalamic gray matter (THA), and occipital white matter (OWM) regions [1] of the quantitative fetal brain R_2^* maps using the arrayShow [56] tool implemented in MATLAB (MathWorks, Natick, MA). Bland–Altman analyses were used to compare ROI-based mean quantitative values between reference and the proposed method.

Results

We first validated the proposed technique on a numerical phantom, which offers a broad range of ground-truth quantitative values under noisy conditions. Figure 1 (top) shows water, fat, R_2^* , and B_0 maps obtained from the model-based reconstruction with a 2-second multi-echo radial FLASH acquisition. Figure 1 (bottom) compares ROI-analyzed quantitative values with the ground truth. The mean differences are 0.03 ± 0.3 s⁻¹ and 0.02 ± 0.07 Hz for R_2^* , and B_0 , respectively. The low mean differences indicate good quantitative accuracy of the proposed method.

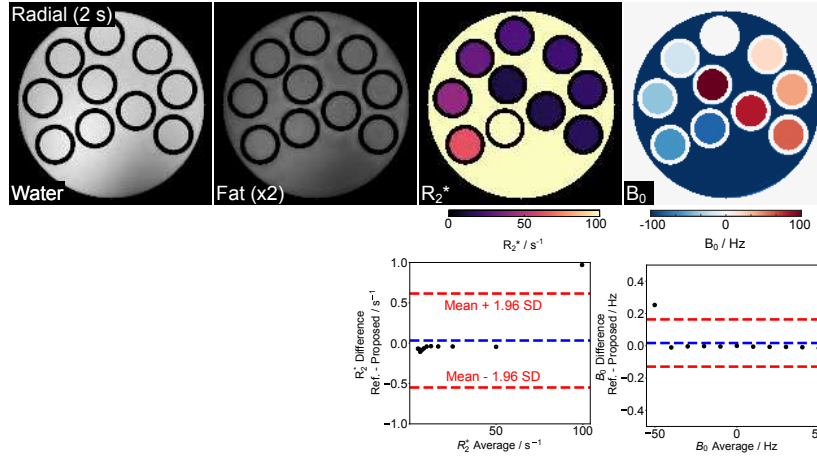


Figure 1. (Top) Model-based estimated water, fat ($\times 2$), R_2^* , and B_0 field maps using a 2-second multi-echo radial FLASH sequence for a numerical phantom. (Bottom) Bland-Altman plots comparing the ROI-analyzed mean quantitative values to the ground truth. The mean differences are $0.03 \pm 0.3 \text{ s}^{-1}$ and $0.02 \pm 0.07 \text{ Hz}$ for R_2^* and B_0 , respectively.

Figure 2 presents NIST R_2^* (top) and B_0 (bottom) maps generated by the proposed method and a 3D Cartesian reference. Note that here a 3-parameter model (i.e., excluding fat in Equation 1) was employed in the reconstruction as there is no known fat component in the NIST phantom. Despite phase wrap differences around the central top two tubes on the B_0 maps, both visual inspection and quantitative ROI analysis demonstrate good agreement: The mean R_2^* difference is $0.6 \pm 2.4 \text{ s}^{-1}$ for R_2^* ranging from 4 s^{-1} to 60 s^{-1} .

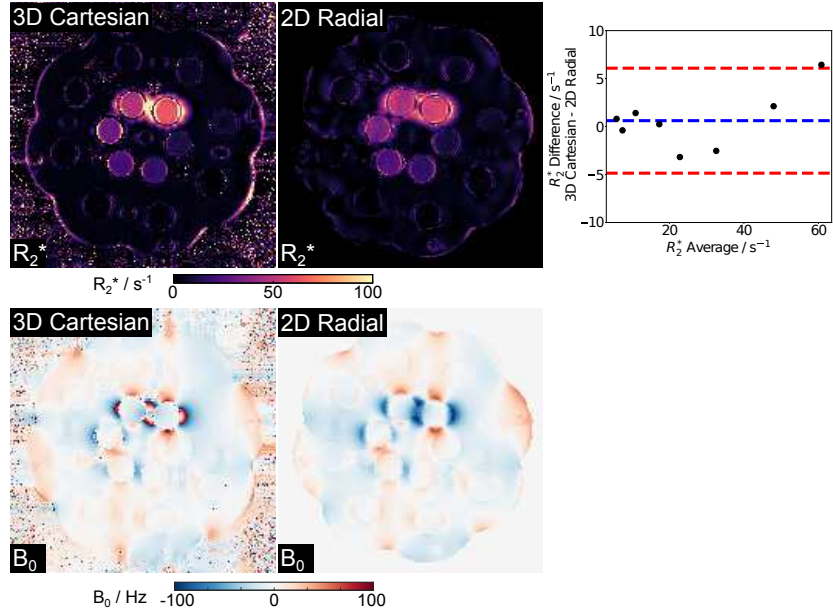


Figure 2. Model-based estimated (top) R_2^* and (bottom) B_0 maps and their comparison to the 3D Cartesian references of the NIST phantom (T1 sphere). (Top right) Bland–Altman plots comparing the ROI-analyzed mean quantitative R_2^* values to the references. The mean difference is $0.6 \pm 2.8 \text{ s}^{-1}$. Note that the 3D Cartesian reference acquisition time is 4:17 min, while the 2D radial sequence requires 2 seconds per slice.

Figure 3 (A) shows reconstructed water, fat, R_2^* , and B_0 maps obtained using the proposed model-based method and a PICS reconstruction with the Graph Cut technique on the same radial dataset. Visual inspection indicates good correspondence between the two methods. Figure 3 (B) includes enlarged R_2^* maps, synthesized R_2^* -weighted images at $TE = 60 \text{ ms}$, and Bland-Altman plots comparing mean R_2^* values for selected ROIs (white circles). Despite the proposed model-based method showing a better balance between preserving fine details and reducing noise in both R_2^* maps and synthesized R_2^* -weighted images (black arrows), the low mean difference ($0.07 \pm 0.17 \text{ s}^{-1}$) confirms strong quantitative agreement. The above findings are further supported by comparisons across four additional subjects and quantitative results shown in Figure 4. Figure 4 (A) highlights comparable image quality with enhanced details in the model-based reconstruction (white and black arrows), while Figure 4 (B) demonstrates small quantitative differences between the two reconstruction approaches.

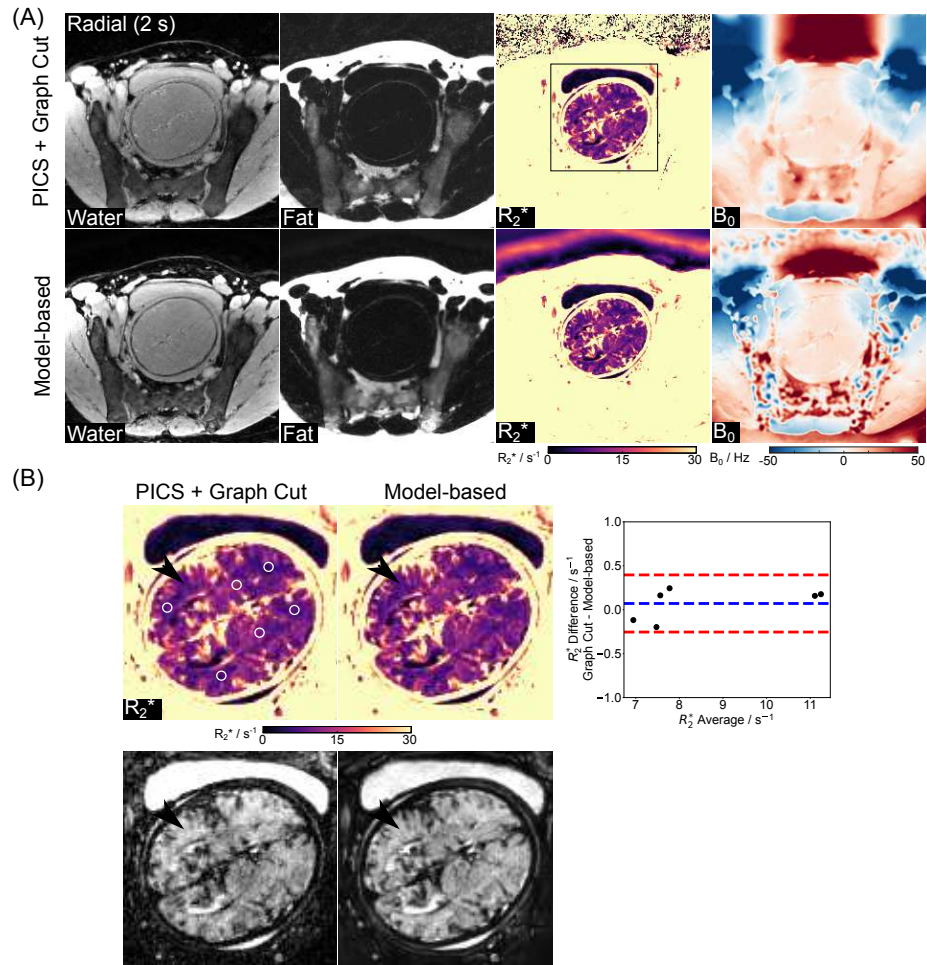


Figure 3. (A). Model-based reconstructed water, fat, R_2^* , and B_0 maps and their comparison to a reference method (Parallel imaging compressed sensing with Graph Cut) utilizing the same radial data. (B). Enlarged R_2^* maps and R_2^* -weighted images (TE = 60 ms) and the Bland–Altman plots comparing the ROI-analyzed (white circles) mean quantitative R_2^* values. The mean difference is $0.07 \pm 0.17 \text{ s}^{-1}$ for all ROIs. Black arrows indicate a better balance between preserving fine details and reducing noise of the model-based approach.

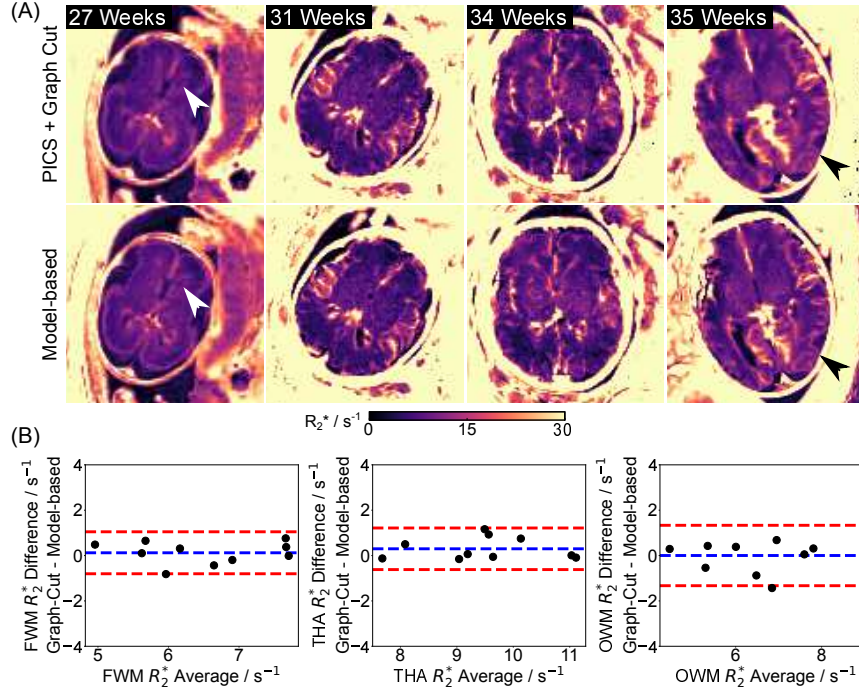


Figure 4. (A). Comparison of quantitative fetal brain R_2^* maps estimated using (top) PICS with Graph Cut and (bottom) model-based reconstruction for the other four subjects. White and black arrows indicate improved image details by model-based reconstruction. (B). Bland–Altman plots comparing the mean quantitative R_2^* values for all five subjects. The mean R_2^* differences for FWM, THA and OWM are $0.12 \pm 0.47 s^{-1}$, $0.30 \pm 0.47 s^{-1}$, and $0.002 \pm 0.68 s^{-1}$, retrospectively.

Figure 5 presents estimated radial water, R_2^* , and B_0 maps with model-based reconstruction, along with EPI M_0 and R_2^* maps and T2-weighted HASTE images for two representative subjects (27 weeks and 36 weeks). Apart from motion-related differences, qualitative assessment demonstrates improved spatial resolution and reduced distortion by the proposed radial technique in both cases. Figure 6 (A) compares quantitative R_2^* maps generated from the radial and EPI techniques for the other three subjects. Consistent with Figure 5, the radial R_2^* maps exhibit higher spatial resolution and less distortion compared to EPI maps. Figure 6 (B) presents ROI-analyzed quantitative values for both methods across all five subjects. The mean differences for FWM, THA and OWM are $-0.2 \pm 1.3 s^{-1}$, $-0.5 \pm 1.0 s^{-1}$, and $0.5 \pm 1.5 s^{-1}$ between radial and EPI approaches. Additionally, Table 1 presents the mean R_2^* values for all subjects. The EPI mean R_2^* values are $6.1 \pm 1.2 s^{-1}$, $8.8 \pm 1.3 s^{-1}$, and $6.9 \pm 1.9 s^{-1}$, while the radial ones are $6.4 \pm 1.0 s^{-1}$, $9.3 \pm 1.1 s^{-1}$, $6.4 \pm 1.3 s^{-1}$ for FWM, THA and OWM, respectively.

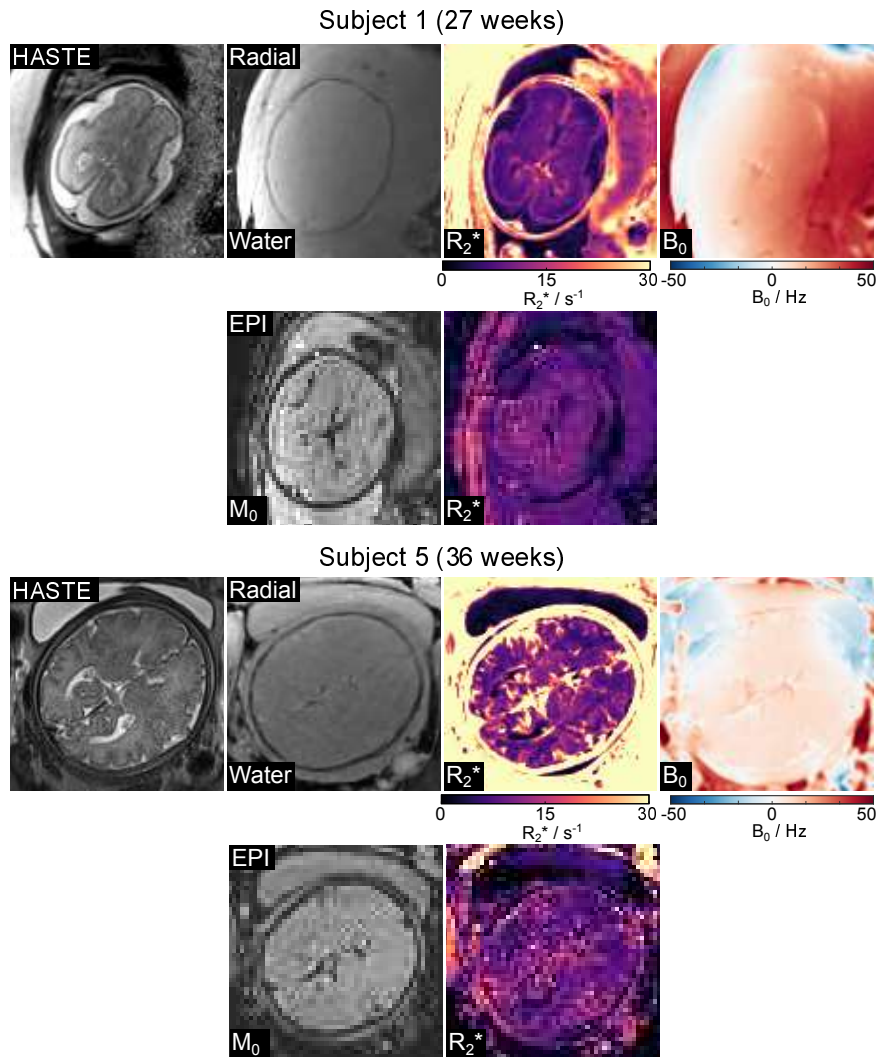


Figure 5. HASTE images, model-based reconstructed water, R_2^* , and B_0 maps, along with a comparison to the EPI results for two representative subjects (27 weeks, top; 36 weeks, bottom). The radial acquisition demonstrates notably improved spatial resolution and reduced distortions compared to the EPI counterpart in both cases.

Table 1: Quantitative R_2^* values (s^{-1} , mean \pm SD) for fetal brains.

Tissue	FWM	THA	OWM
Radial 3T	6.4 ± 1.0	9.3 ± 1.1	6.4 ± 1.3
EPI 3T	6.1 ± 1.2	8.8 ± 1.3	6.9 ± 1.9
Rivkin et al.[4] 1.5 T	6.6	7.9	
Vasylechko et al.[1] 1.5 T	4.3	6.5	4.0
Blazejewska et al.[5] 1.5 T	3.9	6.0	
Vasylechko et al.[9] 3.0 T	5.0	6.6	4.4

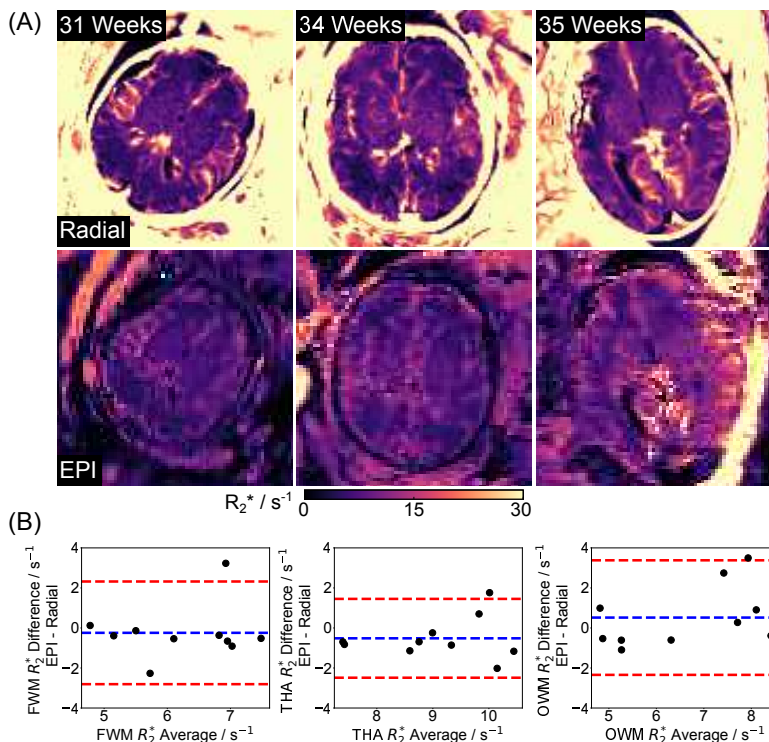
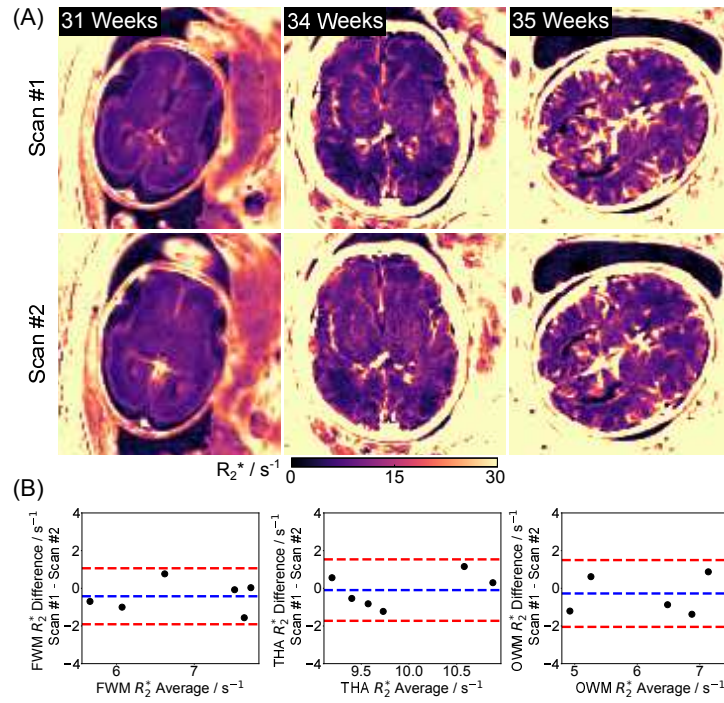


Figure 6. (A). Quantitative R_2^* maps estimated with (top) multi-echo radial FLASH using model-based reconstruction and (bottom) EPI for the other three subjects. (B). Bland–Altman plots comparing ROI mean quantitative R_2^* values between the proposed technique and the EPI method for five subjects, showing a mean difference of $-0.2 \pm 1.3 s^{-1}$, $-0.5 \pm 1.0 s^{-1}$ and $0.5 \pm 1.5 s^{-1}$ for FWM, THA and OWM, respectively.

Supporting Information Figure S2 (A) presents two repetitive fetal brain R_2^* maps for three subjects. Despite varying motion conditions, the quantitative maps appear visually consistent. This observation is confirmed by the minimal quantitative differences observed in the selected ROIs, as shown in Supporting Information Figure S2 (B). In addition to quantitative maps, Figure 7 demon-

strates synthesized R_2^* -weighted images at TE= 70 ms (a typical value chosen for fetal functional MRI study) of the proposed radial approach and EPI methods as well as T2-weighted HASTE images across all subjects. In line with R_2^* images, the contrast-weighted radial images demonstrate improved spatial resolution and reduced distortion compared to EPI. Moreover, the radial FLASH images are less affected by the B1 inhomogeneity than the T2-weighted HASTE images, which could provide additional values for fetal imaging.



Supporting Information Figure S2. (A). Quantitative fetal brain R_2^* maps for two repeated scans across three subjects. (B). The scan-rescan R_2^* differences are $-0.4 \pm 0.8 \text{ s}^{-1}$, $-0.1 \pm 0.8 \text{ s}^{-1}$ and $-0.3 \pm 0.9 \text{ s}^{-1}$ for FWM, THA and OWM.

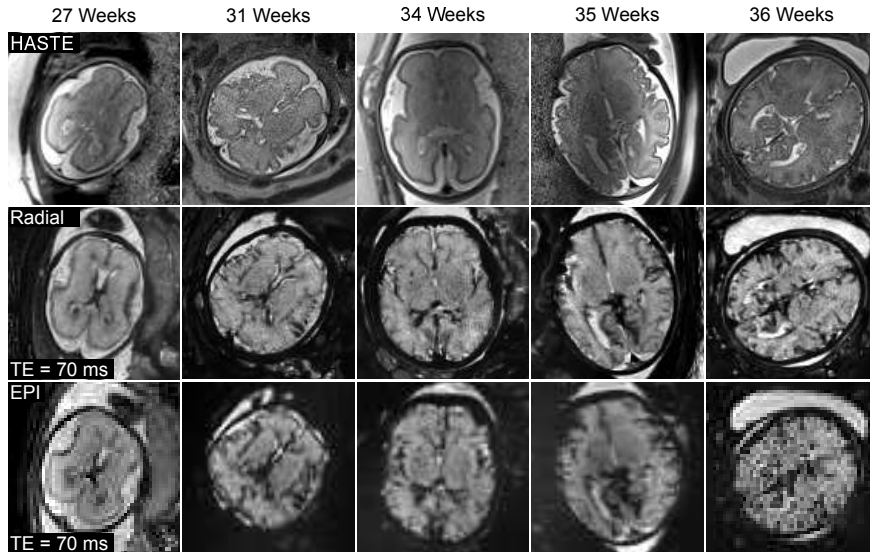
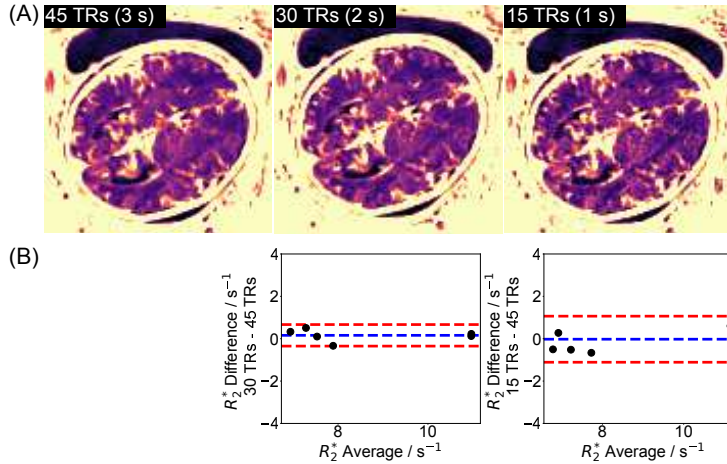


Figure 7. (Top) HASTE images, synthesized R_2^* -weighted images at $TE = 70$ ms for (middle) radial and (bottom) EPI acquisitions. The nominal spatial resolution for HASTE, radial FLASH and EPI are $1.0 \times 1.0 \times 2$ mm³, $1.1 \times 1.1 \times 3$ mm³, and $2\text{-}3 \times 2\text{-}3 \times 3$ mm³, respectively.

The supporting information videos S1 and S2 provide the estimated radial R_2^* maps and corresponding synthesized R_2^* -weighted images at $TE = 70$ ms for 20 slices of the same subjects shown in Figure 5 (i.e., Subject 1: 27 weeks, Subject 5: 36 weeks). The datasets were acquired in a slice-interleaved manner and reordered for video formatting. While S1 demonstrates the proposed radial approach can produce high-resolution R_2^* maps and contrast-weighted images for a fetal brain with rapid motion, S2 shows high-resolution R_2^* maps and images can be readily achieved by the proposed approach when the fetal brain remains more stable.



Supporting Information Figure S3. (A). Quantitative R_2^* maps for Subject 5 estimated using 3-second (45 TRs), 2-second (30 TRs), and 1-second (15 TRs) multi-echo radial FLASH acquisitions. Because of minimal motion during data acquisition, the 2-second and 1-second data were retrospectively undersampled from the 3-second one. (B) Bland-Altman plots comparing mean R_2^* values between the 3-second and 2-second, and 3-second and 1-second acquisitions. The mean difference are $0.16 \pm 0.26 \text{ s}^{-1}$ and $-0.02 \pm 0.6 \text{ s}^{-1}$, respectively.

Discussion

In this work, we present a rapid, high-resolution, and distortion-free R_2^* mapping technique for the fetal brain. With the multi-echo radial sequence offering motion robustness and efficient k-space coverage, the regularized calibration-less model-based reconstruction efficiently estimates quantitative maps and coil sensitivity maps directly from undersampled k-space data. Validation through simulations, phantom studies, and data from five fetal subjects confirms reliable and accurate R_2^* measurements compared to reference methods. This proposed approach achieves distortion-free R_2^* mapping of fetal brain at a nominal resolution of $1.1 \times 1.1 \times 3 \text{ mm}^3$ within 2 seconds. Furthermore, the developed method enables the generation of high-resolution R_2^* -weighted images, offering complementary information to the conventional T2-weighted HASTE images for fetal imaging.

To the best of our knowledge, this is the first study utilizing motion-robust 2D radial acquisition for rapid, high-resolution, and distortion-free R_2^* mapping of the fetal brain. The proposed radial method shows improved spatial resolution and reduced distortion than the conventional multi-echo EPI approaches for all cases. Despite differences in fetal position, spatial resolution and distortions between these two acquisition strategies, quantitative results demonstrate a good agreement between the two. Moreover, our results indicate both the PICS with Graph Cut and model-based reconstruction are effective

for parameter quantification. Although PICS with graph cut is considered the state-of-the-art method for quantification of R_2^* and B_0 in body imaging, the model-based approach offers enhanced image details by directly reconstructing parameter maps from k-space with direct regularization applied to quantitative R_2^* maps. Compared to the values in the literature, the present R_2^* values (both radial and EPI) are slightly higher, especially for the THA regions. This could be due to the age difference in the studied fetal groups as R_2^* values change rapidly along the gestation age. A more detailed analysis of R_2^* variation across age and between subjects warrants a larger scale study, which requires enrolling and scanning a larger number of subjects.

Stack-of-stars radial multi-echo acquisitions [21] have been employed for 3D R_2^* mapping of the placenta [27], and our previous work extended this approach to fetal brain R_2^* mapping [57]. While these 3D methods perform well for fetal brains with minimal or no motion, they require extended acquisition times (over 3 minutes), posing challenges in cases of rapid fetal brain motion, even with advanced motion correction techniques. In contrast, the proposed 2D technique delivers reliable R_2^* maps within a short acquisition window, demonstrating robustness in scenarios with significant fetal motion. Moreover, the proposed method is very general and can be extended to the quantification of other challenging fetal organs. For instance, high-resolution quantitative R_2^* mapping of the fetal liver is of great interest as it could provide valuable insights into evaluating liver iron overload in the fetal stage.

As a technical development study, this work is limited by the relatively small number of subjects. Moreover, repeatability could only be assessed for 3 out of 5 subjects due to limited scan time during the development phase. Future studies will apply the technique to a larger cohort to investigate brain development, focusing on how R_2^* values change across gestational ages. Repeated scans will also be conducted on more subjects to comprehensively evaluate the technique’s repeatability. Furthermore, the 2-second acquisition time, while effective, remains longer than the HASTE sequence. The latter typically takes less than 1 second and is highly effective at freezing motion. Consequently, although the proposed radial acquisition is robust to motion, this method may still be affected by very rapid motion during data acquisition. Our retrospective analysis of Subject 5 (Supporting Information Figure S3) demonstrates that the proposed method can produce reasonable images within 1 second, albeit with increased noise and reduced R_2^* accuracy. To address this, future work will focus on further reducing acquisition time without compromising accuracy or precision. One potential approach would be to replace the hand-crafted ℓ_1 -Wavelet transform with a deep-learning-enhanced regularizer [58] in the model-based reconstruction. Another idea would be to adapt radial simultaneous multi-slice techniques [59] for sub-second quantitative fetal brain imaging.

Conclusion

This work demonstrates the feasibility of radial acquisition for motion-robust quantitative R_2^* mapping of the fetal brain. By combining multi-echo radial FLASH with calibrationless model-based reconstruction, the proposed method achieves accurate, distortion-free fetal brain R_2^* mapping at a nominal resolution of $1.1 \times 1.1 \times 3 \text{ mm}^3$ within 2 seconds.

Conflict of Interest

Dr. Hongli Fan is an employee of Siemens.

Open Research

Data Availability Statement

In the spirit of reproducible research, code and data to reproduce the reconstruction and analysis in this work will be available on <https://github.com/IntelligentImaging/FetalR2Star>.

Acknowledgements

This work was supported by National Institutes of Health (NIH) under award numbers R01NS106030, R01EB031849, R01EB032366, R01HD109395, R01EB032708 and U24EB029240; in part by the Office of the Director of the NIH under award number S10OD025111, R01LM013608, R01EB019483, R01NS133228, R01NS121657 and in part by NVIDIA Corporation. We are grateful to Dr. Ellen Grant for the insightful comments and Dr. Borjan Gagoski for sharing the NIST phantom.

References

- [1] Vasylechko S, Malamateniou C, Nunes RG, Fox M, Allsop J, Rutherford M, Rueckert D, Hajnal JV. T2* relaxometry of fetal brain at 1.5 Tesla using a motion tolerant method. *Magn. Reson. Med.* 2015; 73:1795–1802.
- [2] Sanapo L, Whitehead MT, Bulas DI, Ahmadzia HK, Pesacreta L, Chang T, du Plessis A. Fetal intracranial hemorrhage: role of fetal MRI. *Prenat. Diagn.* 2017; 37:827–836.
- [3] Epstein K, KlineFath B, Zhang B, Venkatesan C, Habli M, Dowd D, Nagaraj U. Prenatal evaluation of intracranial hemorrhage on fetal MRI: a retrospective review. *Am. J. Neuroradiol.* 2021; 42:2222–2228.
- [4] Rivkin M, Wolraich D, Als H, McAnulty G, Butler S, Conneman N, Fischer C, Vajapeyam S, Robertson R, Mulkern R. Prolonged T2* values in

newborn versus adult brain: Implications for fMRI studies of newborns. *Magn. Reson. Med.* 2004; 51:1287–1291.

- [5] Blazejewska AI, Seshamani S, McKown SK, Caucutt JS, Dighe M, Gatenby C, Studholme C. 3D in utero quantification of T2* relaxation times in human fetal brain tissues for age optimized structural and functional MRI. *Magn. Reson. Med.* 2017; 78:909–916.
- [6] Zhao Z, Shuai Y, Wu Y, Xu X, Li M, Wu D. Age-dependent functional development pattern in neonatal brain: an fMRI-based brain entropy study. *NeuroImage* 2024; p. 120669.
- [7] Gholipour A, Estroff JA, Barnewolt CE, Robertson RL, Grant PE, Gagoski B, Warfield SK, Afacan O, Connolly SA, Neil JJ et al. Fetal MRI: a technical update with educational aspirations. *Concepts. Magn. Reson. Part A* 2014; 43:237–266.
- [8] Calixto C, Taymourtash A, Karimi D, Snoussi H, VelascoAnnis C, Jaimes C, Gholipour A. Advances in fetal brain imaging. *Magn. Reson. Imaging Clin.* 2024; 32:459–478.
- [9] Vasylechko S, Hughes E, Allsop J, Fox M, Rueckert D, Hajnal J. Fetal and neonatal whole brain T2* mapping at 3T. In: *Proc. Intl. Soc. Mag. Reson. Med., Virtual*, 2020. p. 0095.
- [10] Afacan O, Estroff JA, Yang E, Barnewolt CE, Connolly SA, Parad RB, Mulkern RV, Warfield SK, Gholipour A. Fetal echo-planar imaging: promises and challenges. *Top. Magn. Reson. Imaging* 2019; 28:245–254.
- [11] Turk EA, Stout JN, Feldman HA, Gagoski B, Zhou C, Tamen R, Manhard MK, Adalsteinsson E, Roberts DJ, Golland P et al. Change in T2* measurements of placenta and fetal organs during Braxton Hicks contractions. *Placenta* 2022; 128:69–71.
- [12] Nichols ES, AlSaoud S, de Vrijer B, McKenzie CA, Eagleson R, de Ribaupierre S, Duerden EG. T2* Mapping of Placental Oxygenation to Estimate Fetal Cortical and Subcortical Maturation. *JAMA Netw. Open* 2024; 7:e240456–e240456.
- [13] Zhang CY, Cleri M, Woodgate T, RamirezGilliland P, Bansal S, AvilesVerdera J, Uus AU, Kyriakopoulou V, StClair K, Story L et al. Structural and functional fetal cardiac imaging using low field (0.55 T) MRI. *Front. Pediatr.* 2024; 12:1418645.
- [14] AvilesVerdera J, Story L, Hall M, Finck T, Egloff A, Seed PT, Malik SJ, Rutherford MA, Hajnal JV, TomiTricot R et al. Reliability and feasibility of low-field-strength fetal MRI at 0.55 T during pregnancy. *Radiology* 2023; 309:e223050.

- [15] Payette K, Uus AU, Verdera JA, Hall M, Egloff A, Deprez M, TomiTricot R, Hajnal JV, Rutherford MA, Story L et al. Fetal body organ T2* relaxometry at low field strength (FOREST). *Med. Image Anal.* 2024; p. 103352.
- [16] Wang F, Dong Z, Reese TG, Bilgic B, KatherineManhard M, Chen J, Polimeni JR, Wald LL, Setsompop K. Echo planar time-resolved imaging (EPTI). *Magn. Reson. Med.* 2019; 81:3599–3615.
- [17] Story L, Uus A, Hall M, Payette K, Bakalis S, Arichi T, Shennan A, Rutherford M, Hutter J. Functional assessment of brain development in fetuses that subsequently deliver very preterm: An MRI pilot study. *Prenat. Diagn.* 2024; 44:49–56.
- [18] Peters DC, Korosec FR, Grist TM, Block WF, Holden JE, Vigen KK, Mistretta CA. Undersampled projection reconstruction applied to MR angiography. *Magn. Reson. Med.* 2000; 43:91–101.
- [19] Block KT, Uecker M, Frahm J. Undersampled radial MRI with multiple coils. Iterative image reconstruction using a total variation constraint. *Magn. Reson. Med.* 2007; 57:1086–1098.
- [20] Feng L, Grimm R, Block KT, Chandarana H, Kim S, Xu J, Axel L, Sodickson DK, Otazo R. Golden-angle radial sparse parallel MRI: Combination of compressed sensing, parallel imaging, and golden-angle radial sampling for fast and flexible dynamic volumetric MRI. *Magn. Reson. Med.* 2014; 72:707–717.
- [21] Block KT, Chandarana H, Milla S, Bruno M, Mulholland T, Fatterpekar G, Hagiwara M, Grimm R, Geppert C, Kiefer B. Towards routine clinical use of radial stack-of-stars 3d gradient-echo sequences for reducing motion sensitivity. *J. Korean Soc. Magn. Reson. Med.* 2014; 18:87–106.
- [22] Kecskemeti S, Samsonov A, Velikina J, Field AS, Turski P, Rowley H, Lainhart JE, Alexander AL. Robust motion correction strategy for structural MRI in unsedated children demonstrated with three-dimensional radial MPnRAGE. *Radiology* 2018; 289:509–516.
- [23] Armstrong T, Ly KV, Murthy S, Ghahremani S, Kim GHJ, Calkins KL, Wu HH. Free-breathing quantification of hepatic fat in healthy children and children with nonalcoholic fatty liver disease using a multi-echo 3-D stack-of-radial MRI technique. *Pediatr. Radiol.* 2018; 48:941–953.
- [24] Hu HH, Benkert T, Jones JY, McAllister AS, Rusin JA, Krishnamurthy R, Block KT. 3D T1-weighted contrast-enhanced brain MRI in children using a fat-suppressed golden angle radial acquisition: an alternative to Cartesian inversion-recovery imaging. *Clin. Imaging* 2019; 55:112–118.

- [25] Liu J, Glenn OA, Xu D. Fast, free-breathing, in vivo fetal imaging using time-resolved 3D MRI technique: preliminary results. *Quant. Imaging. Med. Surg.* 2014; 4:123.
- [26] Sun T, Jiang L, Zhang Z, Zhang C, Zhang H, Wang G, Qian Z. Feasibility of free-breathing T1-weighted 3D radial VIBE for fetal MRI in various anomalies. *Magn. Reson. Imaging* 2020; 69:57–64.
- [27] Armstrong T, Liu D, Martin T, Masamed R, Janzen C, Wong C, Chanlaw T, Devaskar SU, Sung K, Wu HH. 3D R2* mapping of the placenta during early gestation using free-breathing multi-echo stack-of-radial MRI at 3T. *J. Magn. Reson. Imaging* 2019; 49:291–303.
- [28] Benkert T, Feng L, Sodickson DK, Chandarana H, Block KT. Free-breathing volumetric fat/water separation by combining radial sampling, compressed sensing, and parallel imaging. *Magn. Reson. Med.* 2017; 78:565–576.
- [29] Schneider M, Benkert T, Solomon E, Nickel D, Fenchel M, Kiefer B, Maier A, Chandarana H, Block KT. Free-breathing fat and R2* quantification in the liver using a stack-of-stars multi-echo acquisition with respiratory-resolved model-based reconstruction. *Magn. Reson. Med.* 2020; 84:2592–2605.
- [30] Tan Z, UnterbergBuchwald C, Blumenthal M, Scholand N, Schaten P, Holme C, Wang X, Raddatz D, Uecker M. Free-breathing liver fat, R2* and B0 field mapping using multi-echo radial FLASH and regularized model-based reconstruction. *IEEE Trans. Med. Imaging* 2023; 42:1374–1387.
- [31] Zhong X, Nickel MD, Kannengiesser SA, Dale BM, Han F, Gao C, Shih SF, Dai Q, Curiel O, Tsao TC et al. Accelerated free-breathing liver fat and R2* quantification using multi-echo stack-of-radial MRI with motion-resolved multidimensional regularized reconstruction: Initial retrospective evaluation. *Magn. Reson. Med.* 2024; 92:1149–1161.
- [32] Petzschner FH, Ponce IP, Blaimer M, Jakob PM, Breuer FA. Fast MR parameter mapping using k-t principal component analysis. *Magn. Reson. Med.* 2011; 66:706–716.
- [33] Huang C, Graff CG, Clarkson EW, Bilgin A, Altbach MI. T2 mapping from highly undersampled data by reconstruction of principal component coefficient maps using compressed sensing. *Magn. Reson. Med.* 2012; 67:1355–1366.
- [34] Zhao B, Lu W, Hitchens TK, Lam F, Ho C, Liang ZP. Accelerated MR parameter mapping with low-rank and sparsity constraints. *Magn. Reson. Med.* 2015; 74:489–498.

- [35] Tamir JI, Uecker M, Chen W, Lai P, Alley MT, Vasanawala SS, Lustig M. T2 shuffling: Sharp, multicontrast, volumetric fast spin-echo imaging. *Magn. Reson. Med.* 2017; 77:180–195.
- [36] Block KT, Uecker M, Frahm J. Model-Based Iterative Reconstruction for Radial Fast Spin-Echo MRI. *IEEE Trans. Med. Imaging* 2009; 28:1759–1769.
- [37] Fessler JA. Model-based image reconstruction for MRI. *IEEE Signal Process. Mag.* 2010; 27:81–89.
- [38] Wang X, Tan Z, Scholand N, Roeloffs V, Uecker M. Physics-based reconstruction methods for magnetic resonance imaging. *Philos. Trans. R. Soc. A* 2021; 379:20200196.
- [39] Scholand N, Wang X, Roeloffs V, Rosenzweig S, Uecker M. Quantitative MRI by nonlinear inversion of the Bloch equations. *Magn. Reson. Med.* 2023; 90:520–538.
- [40] Lustig M, Donoho D, Pauly JM. Sparse MRI: The application of compressed sensing for rapid MR imaging. *Magn. Reson. Med.* 2007; 58:1182–1195.
- [41] Schneider M, Benkert T, Solomon E, Nickel D, Fenchel M, Kiefer B, Maier A, Chandarana H, Block KT. Free-breathing fat and R_2^* quantification in the liver using a stack-of-stars multi-echo acquisition with respiratory-resolved model-based reconstruction. *Magn. Reson. Med.* 2020; 84:2592–2605.
- [42] Tan Z, Voit D, Kollmeier JM, Uecker M, Frahm J. Dynamic water/fat separation and inhomogeneity mapping adjoint estimation using undersampled triple-echo multi-spoke radial FLASH. *Magn. Reson. Med.* 2019; 82:1000–1011.
- [43] Wundrak S, Paul J, Ulrici J, Hell E, Geibel MA, Bernhardt P, Rottbauer W, Rasche V. Golden ratio sparse MRI using tiny golden angles. *Magn. Reson. Med.* 2016; 75:2372–2378.
- [44] Wang X, Scholand N, Tan Z, Mackner D, Telezki V, Blumenthal M, Schaten P, Uecker M. Model-Based Reconstruction for Joint Estimation of T1, R2* and B0 Field Maps Using Single-Shot Inversion-Recovery Multi-Echo Radial FLASH. *arXiv preprint arXiv:2402.05366* 2024; .
- [45] Yu H, Shimakawa A, McKenzie CA, Brodsky E, Brittain JH, Reeder SB. Multiecho water-fat separation and simultaneous R2* estimation with multifrequency fat spectrum modeling. *Magn. Reson. Med.* 2008; 60:1122–1134.
- [46] Pruessmann KP, Weiger M, Scheidegger MB, Boesiger P. SENSE: sensitivity encoding for fast MRI. *Magn. Reson. Med.* 1999; 42:952–962.

- [47] Uecker M, Hohage T, Block KT, Frahm J. Image reconstruction by regularized nonlinear inversion-joint estimation of coil sensitivities and image content. *Magn. Reson. Med.* 2008; 60:674–682.
- [48] Wang X, Roeloffs V, Klosowski J, Tan Z, Voit D, Uecker M, Frahm J. Model-based T1 mapping with sparsity constraints using single-shot inversion-recovery radial FLASH. *Magn. Reson. Med.* 2018; 79:730–740.
- [49] Uecker M, Ong F, Tamir JI, Bahri D, Virtue P, Cheng JY, Zhang T, Lustig M. Berkeley advanced reconstruction toolbox. In: *Proc. Intl. Soc. Mag. Reson. Med., Toronto, 2015.* p. 2486.
- [50] Stupic KF, Ainslie M, Boss MA, Charles C, Dienstfrey AM, Evelhoch JL, Finn P, Gimbutas Z, Gunter JL, Hill DL et al. A standard system phantom for magnetic resonance imaging. *Magn. Reson. Med.* 2021; 86:1194–1211.
- [51] Rosenzweig S, Holme HCM, Uecker M. Simple auto-calibrated gradient delay estimation from few spokes using Radial Intersections (RING). *Magn. Reson. Med.* 2019; 81:1898–1906.
- [52] Wajer FTAW, Pruessmann KP. Major speedup of reconstruction for sensitivity encoding with arbitrary trajectories. In: *Proc. Intl. Soc. Mag. Reson. Med., Glasgow, 2001.* p. 0767.
- [53] Uecker M, Zhang S, Voit D, Karaus A, Merboldt KD, Frahm J. Real-time MRI at a resolution of 20 ms. *NMR Biomed.* 2010; 23:986–994.
- [54] Hernando D, Kellman P, Haldar J, Liang ZP. Robust water/fat separation in the presence of large field inhomogeneities using a graph cut algorithm. *Magn. Reson. Med.* 2010; 63:79–90.
- [55] Hu HH, Börnert P, Hernando D, Kellman P, Ma J, Reeder SB, Sirin C. ISMRM workshop on fat-water separation: Insights, applications and progress in MRI. *Magn. Reson. Med.* 2012; 68:378–388.
- [56] Sumpf T, Unterberger M. arrayshow: a guide to an open source matlab tool for complex MRI data analysis. In: *Proc. Intl. Soc. Mag. Reson. Med., Salt Lake City, 2013.* p. 2719.
- [57] Wang X, Wang J, Afacan O, Vasylechko S, Warfield S, Gholipour A. Quantitative T2* and B0 Mapping of Fetal Brain Using Stack-of-Star Multi-Echo FLASH and Model-Based Reconstruction . In: *Proc. Intl. Soc. Mag. Reson. Med., Singapore, 2024.* p. 0823.
- [58] Blumenthal M, Fantinato C, UnterbergBuchwald C, Haltmeier M, Wang X, Uecker M. Self-supervised learning for improved calibrationless radial MRI with NLINV-Net. *Magn. Reson. Med.* 2024; 92:2447–2463.
- [59] Wang X, Rosenzweig S, Scholand N, Holme HCM, Uecker M. Model-based reconstruction for simultaneous multi-slice T1 mapping using single-shot inversion-recovery radial FLASH. *Magn. Reson. Med.* 2021; 85:1258–1271.